Eur. Phys. J. A **12**, 199–205 (2001)

THE EUROPEAN PHYSICAL JOURNAL A

Incomplete fusion reactions: Analysis of excitation functions and recoil range distributions in $^{16}O + ^{51}V$

S. Mukherjee[1,a], A. Sharma[1], S. Sodaye[2], B.S. Tomar[2], A. Goswami[2], and S.B. Manohar[2]

[1] School of Studies in Physics, Vikram University, Ujjain 456 010, India
[2] Radiochemistry Division, Bhabha Atomic Research Centre, Mumbai 400 085, India

Received: 20 June 2001 / Revised version: 5 September 2001
Communicated by W.F. Henning

Abstract. Incomplete fusion reactions were investigated by measuring the excitation functions of nine evaporation residues in $^{16}O + ^{51}V$ reaction in the beam energy 4–6 MeV/amu, using the well-known recoil catcher technique and gamma-ray spectrometry. The experimental data were compared with that obtained from Monte Carlo simulation calculations using the PACE2 code. The results indicate the presence of incomplete fusion process in the production of two alpha emission products. This was further confirmed by the measurement of recoil range distribution of these isotopes at 96 MeV beam energy. Calculations of the average angular momentum associated with these products revealed the peripheral nature of these ICF reactions.

PACS. 25.70.Jj Fusion and fusion-fission reactions – 25.70.Gh Compound nucleus

1 Introduction

The mechanism of the incomplete fusion (ICF) reactions is still not clearly understood, particularly with regards to the angular momentum involved in the process. The studies by Trautmann *et al.* [1] showed that ICF is associated with peripheral collisions, while some studies like that by Tricoire *et al.* [2] suggest the involvement of lower angular momenta than the critical angular momentum for complete fusion (CF) in these reactions. Incomplete fusion can be thought of as a process in which the projectile breaks up near the surface of the target nucleus into two fragments, one of which escapes with relatively unchanged velocity, while the other fuses with the target to form an excited intermediate, which subsequently de-excites, in the usual way, by particle evaporation. However, systematic quantitative measurement of cross-sections are rare.

Bimbot *et al.* [3] carried out the pioneering work on the excitation functions, angular distributions, and differential recoil range to study the transfer of alpha-particle and ^{8}Be, to the target, in $^{12}C + ^{197}Au$ reactions and were able to estimate the total cross-section for each of the transfer process as a function of energy. In recent years this method has been used in studies of complete and incomplete fusion at energies up to 10 MeV/amu. These include ^{12}C on ^{51}V [4], ^{20}Ne and ^{22}Ne on ^{93}Nb [5,6], ^{12}C on ^{89}Y and ^{103}Rh [7,8] and ^{16}O on ^{93}Nb and ^{165}Ho [9,10]. These data have been analyzed in terms of competing transfer reactions. The above studies have shown that for ^{12}C there are three dominant processes: complete fusion, ^{8}Be transfer, and α transfer and that effectively all of the cross-section would be accounted for by these three processes up to an energy of 100 MeV. Similarly, in $^{16}O + ^{89}Y$, the ICF reactions involving the breakup of ^{16}O into $^{12}C + \alpha$ are known.

In this paper, we present our results on experimental measurement of excitation functions of $^{16}O + ^{51}V$ evaporation residues together with the measurement of recoil range distribution (RRD). It is not known whether ICF reactions involving the breakup of ^{16}O into $^{8}Be + ^{8}Be$ also occur at a beam energy range of the present study. The present work is undertaken in order to explain the above points and also to provide new experimental data for the excitation functions in $^{16}O + ^{51}V$, and to estimate the ICF cross-sections at these low bombarding energies.

2 Experimental details

2.1 Measurement of excitation functions

Experiments for the measurement of excitation functions were carried out at BARC-TIFR pelletron accelerator at Mumbai, India. The target samples were irradiated with the collimated ^{16}O beam of diameter 1–2 mm by following

[a] *Present address*: National Accelerator Centre, PO Box 72, Faure 7131, Near Cape Town, South Africa. e-mail: smukherjee@nac.ac.za

Table 1. Decay characteristics of the residual nuclei in $^{16}O + ^{51}V$ reactions.

ERs	Spin	Half-life	E_γ (keV)	I_γ (%)
^{65}Ga	$3/2^-$	15.2 m	115	55
^{63}Zn	$3/2^-$	38.7 m	670	8.4
^{62}Zn	0^+	9.186 h	597	28
^{61}Cu	$3/2^-$	3.3 h	656	10
^{60}Cu	2^+	23.7 m	826	88
^{61}Co	$7/2^-$	1.65 h	908.6	3
^{58}Co	2^+	70.2 d	811	99.4
^{57}Co	$7/2^-$	271.79 d	122	85.5
^{56}Co	4^+	77.2 d	1238	66

the stacked foil activation technique. Stacks consisting of two self-supporting targets of vanadium, each of thickness 2.1 mg/cm^2 and purity ∼99.99%, separated by aluminum foils (∼2 mg/cm^2) were bombarded with an ^{16}O beam. Several irradiations were carried out for each such stack of target and degraders to encompass the ^{16}O beam energy between 58 and 94 MeV. There was thus considerable overlap between various irradiations. The beam energy degradation in each target foil was calculated using the stopping power tables of Northcliffe and Schilling [11].

After the irradiation, the target and the catcher foil were counted in the live time mode in the desired geometry for the gamma activities. The counting geometry was chosen in such a way so that the count rate is appreciable and at the same time the dead time of the detector is $\leqslant$ 10%. A 60 cc HPGe detector coupled to a 4 K MCA having a resolution of 2 KeV at 1332 KeV was used for this purpose. A background spectrum was taken in order to check the presence of any background gamma peak due to contamination of the detector surroundings. The recording time period were chosen in such a way so as to get the good counting statistics. The duration of counting was initially kept in the order of seconds and subsequently increased to longer periods for counting long-lived products. Table 1 indicates the reaction products identified, their characteristic gamma lines with their abundances. The computer code SAMPO was used to find the areas of the peaks in the gamma-ray spectra. From the measured count rate CR(t) at any time t, the cross-sections (σ) were calculated using the standard relation [7]. The yields of the radionuclides identified in each foil were determined using the published half-lives, gamma-ray energies and branching ratios [12].

2.2 Errors in measurement

The errors on the cross-section arise mostly from the counting statistics (1–4%), target thickness (5–8%), detection efficiency (4%), beam fluence (< 5%) and gamma-ray intensity values (5–10%). The errors on the cross-sections are approximately 10–15%.

2.3 Measurement of recoil range distributions

In the measurement of recoil range distributions, thin targets of metallic vanadium, of thickness around 200 μg/cm^2, was mounted with the aluminum backing facing the beam followed by several aluminum catcher foils of thickness around 100 μg/cm^2. The target and catcher assembly was bombarded with ^{16}O at 96 MeV for about 18 hours. The beam current was measured with an electron-suppressed Faraday cup placed behind the target-catcher assembly. Total charge collected during irradiation was 2737 μC. Other details of the experiment are given elsewhere [7,13].

After the irradiation each aluminum catcher foil was counted for the gamma-ray activity of evaporation residues (ERs) in a similar way as described in subsect. 2.1. The short-lived ERs could not be tagged in the RRD measurement owing to the time taken in dismantling the stack of catcher foils and mounting each of them for counting and also large-time gap between two successive countings of the same foil. The counting was continued for a period of 15 days. The gamma-ray spectra were analyzed by the peak-fitting program SAMPO to obtain the peak area (PA). The measured activities were corrected for their decay to obtain the activities at the end of irradiation ($A(T_i)$). For RRD measurement the cross-section measured in each foil was divided by the respective foil thickness (in mg/cm^2) to obtain the normalized cross-section (mb/mg/cm^2) which was plotted against the cumulative catcher thickness to obtain the RRD. The cross-section (σ) for a particular reaction product in different catcher foils and the uncertainty in the cross-section measurements were determined in a similar way as described in the previous section.

3 Experimental results

3.1 Excitation functions of $^{16}O + ^{51}V$ reactions

Figures 1-4 show the excitation functions of nine evaporation residues measured in the present work in $^{16}O + ^{51}V$ reactions. The reaction product ^{65}Ga has only the ground state having half-life of 15.2 minutes and spin $3/2^-$. The decay of this state is through electron capture (EC) mode (100%). Similarly the reaction products $^{62\text{-}63}$Zn also have ground states of half-lives 38.47 minutes and 9.186 hours, with spins $3/2^-$ and 0^+, respectively. The decay of these states is through electron capture mode (100%). The reaction products $^{60\text{-}61}$Cu, which have ground-states of half-lives 23.7 minutes and 3.34 hours, respectively, with spins 2^+ and $3/2^-$, respectively, decay through electron capture. In the present work we have measured the product ^{58}Co which has two states *i.e.* one metastable state with half-life 9.15 hours and spin 5^+, while the ground state is having half-life 70.82 days with spin 2^+. The metastable state of ^{58}Co decays through isomeric transition (IT) (100%). The ground state decays through electron capture mode (100%). In the present work we have measured the total cross-section of ^{58}Co by allowing for the complete decay of

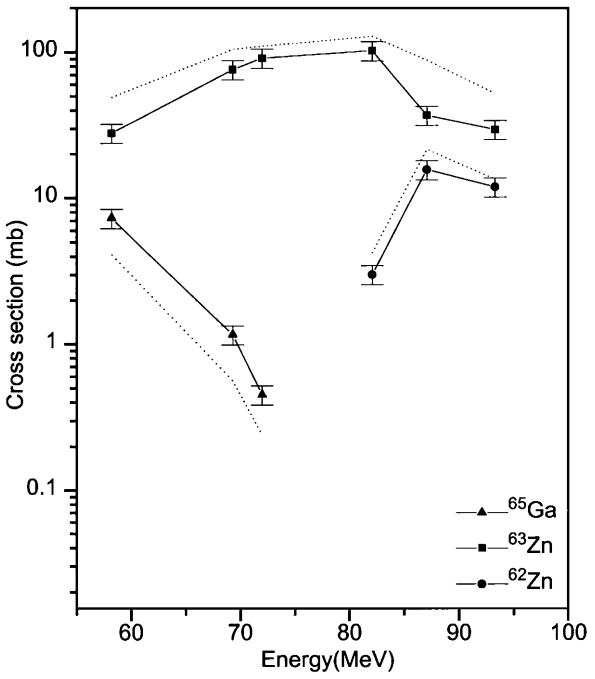

Fig. 1. Excitation functions of ^{65}Ga, ^{63,62}Zn evaporation residues in $^{16}O + ^{51}V$ reaction. The solid lines are guides to the experimental data points. The dotted curves are the results of statistical model calculations using the PACE2 Monte Carlo code.

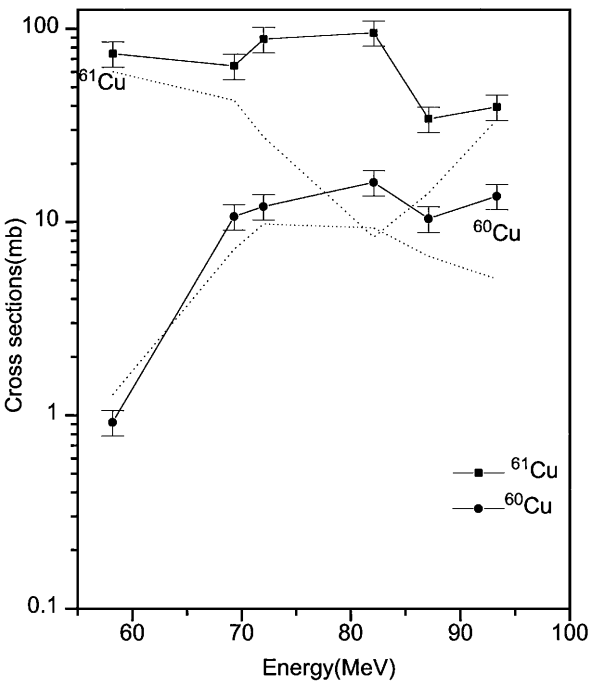

Fig. 2. Excitation functions of ^{61,60}Cu evaporation residues in $^{16}O + ^{51}V$ reaction. Notations as in fig. 1.

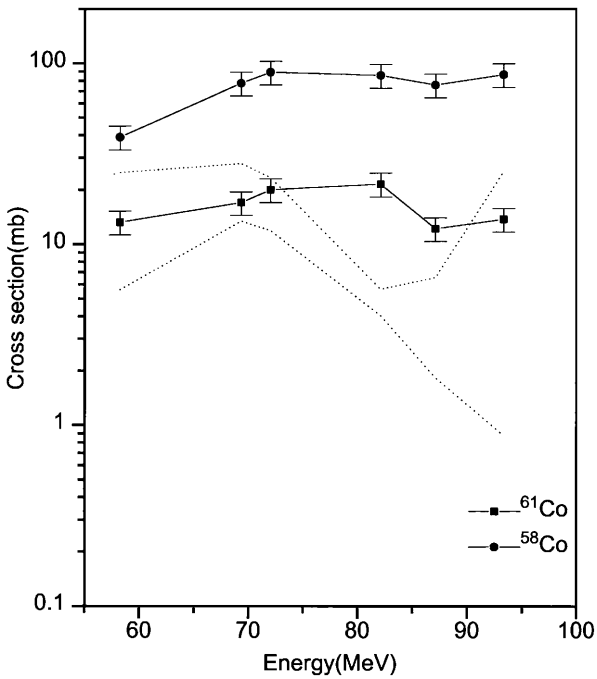

Fig. 3. Excitation functions of ^{61,58}Co evaporation residues in $^{16}O + ^{51}V$ reaction. Notations as in fig. 1.

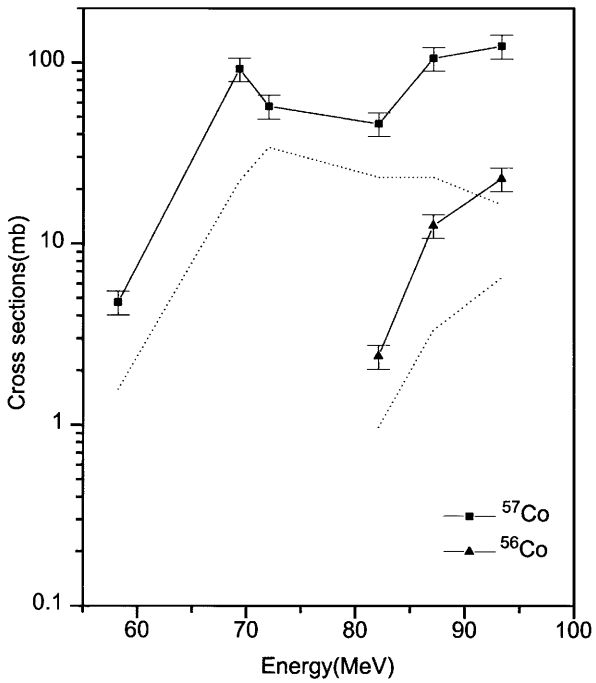

Fig. 4. Excitation functions of ^{57,56}Co evaporation residues in $^{16}O + ^{51}V$ reaction. Notations as in fig. 1.

the isomeric state to the ground state. The presently measured reaction products $^{57\text{-}56}$Co have only ground states with corresponding half-lives 271.79 days and 77.27 days, respectively, and spins $7/2^-$ and 4^+, respectively.

3.2 Comparison with theoretical calculations

Figures 1-4 show the excitation functions of gallium, zinc, copper and cobalt isotopes, respectively formed in $^{16}\mathrm{O} + ^{51}\mathrm{V}$ reaction up to 96 MeV. The theoretical estimate of the cross-sections for evaporation residues formed in the complete fusion were obtained using the Monte Carlo simulation code PACE2 [14] modified to take into account the excitation energy dependence of level density parameter (a) using the prescription of Kataria *et al.* [15]. The optical model parameters for emitted light particles (n, p, α) were taken from Perey and Perey [16]. The average gamma transition strengths compiled by Endt [17] were used for the present work. The fusion cross-sections were calculated following the prescription of Bass [18]. The level density parameter a was taken as $A/8$ MeV^{-1}. The spin cut-off parameter representing the effective moment of inertia was reduced to 0.7 times the rigid body value which resulted in an agreement between the experimental and the calculated data. This is justified as we expect more stretched and deformed compound nucleus configurations and consequently also deformed parent nuclei as the higher angular momenta are involved in these reactions. The other input parameters in the program were used as default values. Owing to a finite sample size in Monte Carlo simulation, the error in the calculated cross-section is about 30%, 10% and 3% for $\sigma = 1$ mb, 10 mb and 100 mb, respectively. The calculated values are shown as dotted curves in the figures.

It can be observed in fig. 1 that the experimental excitation functions are in satisfactory agreement with the calculated ones, expect for the ^{62}Zn isotope where the calculated value is as high as a factor of 2 compared to the experimental value. Within this limitation the results indicate that the evaporation residues ^{65}Ga, $^{63\text{-}62}$Zn are formed in the complete fusion of ^{16}O with ^{51}V by de-excitation of compound nucleus (^{67}Ga) via xn and pxn channels, respectively. Figure 2 shows the excitation functions for the evaporation residues ^{61,60}Cu. While at low energy there is agreement between experimental and calculated results, at higher energy the experimental data are much higher than the calculated ones indicating the contributions of ICF in copper isotopes. This can be explained in terms of the breakup of ^{16}O into $^{12}\mathrm{C} + \alpha$ followed by fusion of ^{12}C with ^{51}V giving ^{63}Cu which may subsequently de-excite by neutron evaporation to give ^{61,60}Cu. At highest energy the experimental cross-section of ^{61}Cu is in agreement with calculations. This may be owing to the onset of 2p4n emission channel from compound nucleus and increasing cross-section of 3n and 4n emission from incompletely fused composite nucleus ^{63}Cu.

In case of cobalt products (figs. 3 and 4), the experimental data are much higher than the calculated data indicating the contribution from incomplete fusion

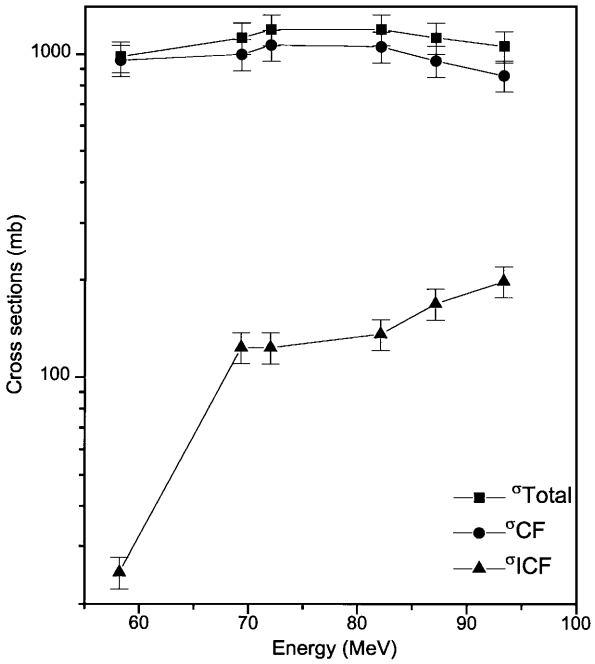

Fig. 5. Excitation functions extracted for the CF and ICF processes along with the total cross-section for the $^{16}\mathrm{O} + ^{51}\mathrm{V}$. The solid lines are guides to the experimental data points.

reactions. These ICF reactions can be of the ^{51}V(^{16}O, ^{8}Be)^{59}Co* type. The excited ^{59}Co* nucleus may subsequently de-excite by neutron emission to give $^{58\text{-}56}$Co. In the case of the evaporation residues ^{61}Co, there may be a breakup of ^{16}O into ^{12}C and ^{4}He and subsequent incomplete fusion of ^{12}C in the reaction ^{51}V(^{16}O, α) ^{63}Cu; the evaporation of two protons leads to the formation of the residues. Figure 5 gives the estimated contributions of the incomplete and complete fusion cross-sections, together with the total reaction cross-section. It was found that the ICF contributions with respect to the CF cross-sections increase from 3% at 60 MeV to about 20% above 90 MeV. Thus, there is a veritable signature of ICF in the enhanced cross-section for the formation of cobalt products. These observations have been further confirmed by measurement of recoil range distribution (RRD) of the evaporation residues in the following section.

3.3 Theoretical calculations of the recoil range distributions: PACE2 analysis

The recoil range distributions for evaporation residues formed in the $^{16}\mathrm{O} + ^{51}\mathrm{V}$ reaction, studied in the present work, were simulated by using the Monte Carlo simulation technique described in PACE2 code. The code calculates the double differential cross-sections ($\mathrm{d}^2\sigma/\mathrm{d}E\mathrm{d}\Omega_{\mathrm{lab}}$) for ERs which was transformed into the projected range distribution along the beam axis using the range energy table of Northcliffe and Schilling [11]. The RRDs obtained by the PACE2 code were normalized to the experimental RRDs by adjusting the height and keeping the peak position and width constant. Since the experimental RRDs

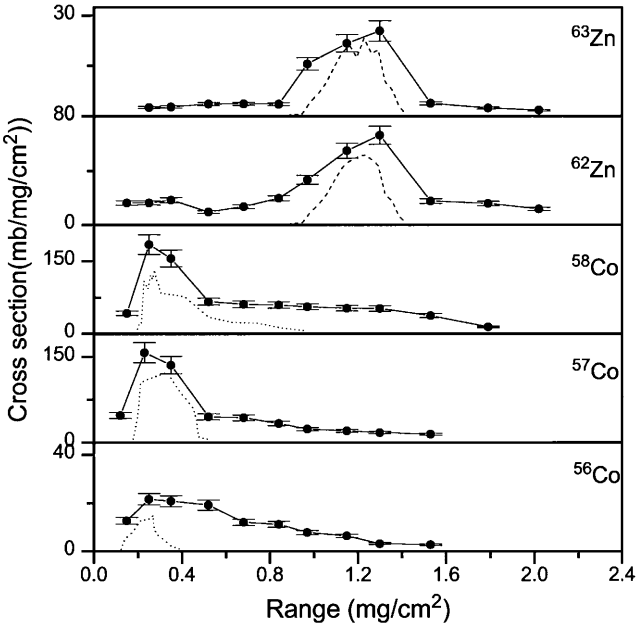

Fig. 6. RRDs of evaporation residues in $^{16}O + ^{51}V$ reaction at 96 MeV. Dashed lines are the PACE2 predictions for CF formation of ERs. Dotted lines are the simulated RRDs for ICF based on the breakup fusion model.

represent the projected recoil ranges along the beam axis, the calculated RRDs were also projected along the $\theta = 0°$ direction.

Figure 6 shows the recoil range distributions of the evaporation residues in the $^{16}O + ^{51}V$ reaction studied in the present work. The RRD of ^{61}Cu and ^{60}Cu could not be measured owing to short half-lives of these isotopes. The simulated RRDs for the evaporation residues obtained by PACE2 calculations are shown by dashed curves for complete fusion. The dash-dotted curves are the ICF components obtained by subtracting CF contributions from the experimental curves. The dotted curves are the simulated ICF components, obtained by breakup fusion model calculations. These figures are discussed in details in the subsequent sections. The spread in RRD data obtained from PACE2 arises due to the process of particle evaporation from the CN and is not expected to reproduce the experimental RRD unless correction due to finite target thickness, non-uniformity of the catcher foil and straggling during stopping are taken into account [19].

3.4 Theoretical interpretation of the recoil range distribution measurements

The recoil range distributions provide information about the extent of linear momentum transfer from projectile in the formation of a particular reaction product. Figure 6 shows the RRDs for five evaporation residues for $^{16}O + ^{51}V$ system at 96 MeV. The RRDs for ^{63,62}Zn isotopes show Gaussian curves with mean range corresponding to full momentum transfer. This shows that the zinc

Table 2. CF and ICF contributions in RRD of $^{16}O + ^{51}V$ reaction (in mb).

Nuclei	CF	ICF
^{62}Zn	14.74 ± 1.37	–
^{61}Zn	48.01 ± 4.065	–
^{58}Co	–	32.75 ± 2.86
^{57}Co	–	27.24 ± 2.56
^{56}Co	–	1.94 ± 0.11

products are mainly produced following the complete fusion of ^{16}O with ^{51}V. Similar inferences were made while explaining the experimental excitation functions of the above products ^{63,62}Zn in terms of theoretical calculations by PACE2 code. The higher-range component in the RRD of $^{56\text{-}58}$Co represents the formation of these evaporation residues by evaporation of two alpha-particles from the compound nucleus, which gives a broad RRD. The theoretical calculation using PACE2 does indicate the formation of the evaporation residues in CF process. For $^{58\text{-}56}$Co isotopes the experimental RRDs also show a lower-range component than that expected for CF, indicating that they are formed in ICF reactions. The possible ICF reactions that can give rise to these products are $^{51}V(^{16}O,^{8}Be)^{59}Co^*$. The excited intermediate nuclei $^{59}Co^*$ may subsequently de-excite by neutron emission to form $^{58\text{-}56}$Co.

This is indicated by the simulated RRD for ICF based on the breakup fusion model as shown in the figure by the dotted curve. The above figures show only the ICF products, with no second peak at the site corresponding to the range of the evaporation residues obtained from complete fusion process. This indicates that the above products are formed predominantly by the breakup of ^{16}O into $^{8}Be + ^{8}Be$ and subsequent fusion of one ^{8}Be into ^{51}V. Similar results of ^{8}Be fusion with the target were obtained by Bindu Kumar *et al.* [7,8]. Table 2 indicates the contribution of CF and ICF in the yields of zinc and cobalt isotopes for the $^{16}O + ^{51}V$ system.

4 Breakup fusion model analysis of ICF for the system $^{16}O + ^{51}V$

In fig. 6 the low-range component clearly reflects incomplete momentum transfer in the ICF process leading to the formation of various incompletely fused composites. The RRD for these ICF products was deduced using the breakup fusion model [20]. The Monte Carlo simulation of RRD was carried out using PACE2 code by supplying the E^* and $\langle \ell \rangle$ of the incompletely fused composite (IFC) nuclei ^{59}Co formed in the binary reaction

$$^{16}O + ^{51}V \longrightarrow ^{59}Co^* + ^{8}Be\,.$$

The E^* of the intermediate nucleus $^{59}Co^*$ was evaluated using the expression,

$$(1/2)E_{\rm lab}(51/59) + Q_{\rm gg}$$

Table 3. Excitation energy (E^*) and average angular momentum $\langle\ell\rangle$ of the ICF (^{59}Co) produced in the $^{16}O + {}^{51}Vo$ at 96 MeV.

E^* (MeV)	$\langle\ell\rangle\hbar$	σ (^{57}Co) (mb)	σ (^{56}Co) (mb)	Ratio	
39	24	80.16	47.12	1.7	
39	25	85.95	42.13	2.04	
39	26	91.23	37.86	2.40	
39	27	95.74	32.12	2.98	
39	28	100.24	28.16	3.55	
38	29	160.23	20.27	7.94	
38	28	155.54	25.29	6.15	
38.5	26	185.32	26.34	6.84	
38.5	25	173.80	24.72	7.03	⟵
37	28	165.62	21.23	7.80	
37	27	160.84	26.23	6.13	
	Experimental	104.24	14.54	7.14	

and was found to be equal to 40.65 MeV at $E_{\rm lab}$ = 96 MeV. The IFC was assumed to have a single spin value equal to 1/2 times the $\ell_{\rm max}$ of the entrance channel, which was found to be 24$\hbar$. The $\ell_{\rm max}$ value for the entrance channel was calculated using the prescription of Wilczynski *et al.* [21] and was found to be 48$\hbar$. The other input parameters were chosen in the same way as in the case of PACE2 calculations for the CF process. The de-excitation of these incompletely fused composites was followed and the RRDs for the cobalt isotopes were generated. The relative cross-sections of $^{58\text{-}56}$Co were used to deduce the E^* and $\langle\ell\rangle$ of the ICF and thereby evaluating the angular momentum involved in the ICF. This method of obtaining the angular-momentum distribution of a compound nucleus from the relative yields of evaporation residues is well established [22]. The E^* and $\langle\ell\rangle$ of the IFC of ^{59}Co were varied in the range of 37–38.5 MeV and 24–29$\hbar$, respectively and the yields of the ^{57}Co and ^{56}Co were compared with experimentally deduced ICF cross-sections for these products. Table 3 gives the values of E^* and $\langle\ell\rangle$ of cobalt isotopes. The best fit with experimental values was found for E^* = 38.5 MeV and $\langle\ell\rangle = 25\hbar$ (indicated by an arrow in the table). These values agree with the prediction of the breakup fusion model as calculated above. The corresponding angular momentum of entrance channel would be $25 \times 2 = 50\hbar$, which agrees with the $\ell_{\rm max}$ value (48$\hbar$) calculated using the prescription of Wilczynski *et al.* [21]. This shows that the ICF process is associated with peripheral collisions. This observation is in agreement with the predictions of the sum rule model [21] that the ICF occurs only in peripheral collisions involving $\ell_{\rm ICF} > \ell_{\rm CF}$ for CF. The CF cross-sections were obtained from the excitation function data measured experimentally in the present work.

Thus the present study has shown that ICF contributes significantly to total reaction cross-section even at as low energy as 6 MeV/amu in case of low-Z heavy-ion–induced reactions. The study reveals that the ICF follows a breakup fusion mechanism in which the projectile breaks into the fragments (^{8}Be + ^{8}Be). Subsequently, either of the two fragments can fuse with the target nucleus bringing in the angular momentum in the ratio of mass to that of the projectile. The calculation of the $\langle\ell\rangle$ of the IFC from the relative yields of the $^{57\text{-}56}$Co isotopes corroborates the peripheral nature of the collision leading to ICF.

5 Conclusions

Excitation functions of nine evaporation residues were measured in$^{16}O + {}^{51}V$ reaction in the beam energy range 4–6 MeV/amu. The recoil range distributions of ^{60,61}Cu could not be measured due to their short half-lives. A comparison with the Monte Carlo simulation code PACE2 shows the enhancement in cross-section for copper and cobalt products thereby indicating the presence of incomplete fusion reactions. In the incomplete fusion reaction, the projectile ^{16}O breaks up into $^{12}C + \alpha$ and ^{8}Be + ^{8}Be followed by fusion of either of the fragment with the target to form ^{63}Cu and ^{59}Co incompletely fused composite nuclei, respectively. This excited nuclei subsequently de-excite by neutron emission to produce ^{61,60}Cu and $^{58\text{-}56}$Co evaporation residues, respectively. The ICF cross-section was found to increase with energy with respect to the complete fusion cross-section. These observations were further supported by the measurements of recoil range distributions. The RRDs measured for the cobalt isotopes contain components that cannot be explained in terms of formation via the compound nucleus in the $^{16}O + {}^{51}V$ reaction but are consistent with the incompletely fused composite ^{59}Co*. The simulation of the RRDs further confirm the occurrence of ICF in the formation of these evaporation residues. The average angular momentum of the incompletely fused products indicates the peripheral nature of the ICF reactions which is in agreement with the predictions of the existing models of incomplete fusion.

The authors (S. Mukherjee and B.S. Tomar) acknowledge the financial help given by the BRNS-DAE, Mumbai, India, through a major research project. Thanks are also due to the target laboratory personnel at TIFR, Mumbai for preparing thin vanadium and aluminum foils for the present experiments. S. Mukherjee thanks Prof. J.F. Sharpey-Schafer and Dr. J.J. Lawrie, National Accelerator Centre, Faure, South Africa, for their help and cooperation.

References

1. W. Trautmann, Ole Hansen, H. Tricoire, W. Hering, R. Ritzka, W. Trombik, Phys. Rev. Lett. **53**, 1630 (1984).
2. H. Tricoire, C. Gerschel, N. Perrin, H. Sergolle, L. Valentin, D. Bachelier, H. Doubre, J. Gizon, Z. Phys. A **306**, 127 (1982).
3. R. Bimbot, D. Gardes, M.F. Rivet, Nucl. Phys. A **189**, 193 (1972).
4. D.J. Parker, J. Asher, T.W. Conlon, I. Naqib, Phys. Rev. C **30**, 143 (1984).
5. D.J. Parker, J.J. Hogan, J. Asher, Phys. Rev. C **31**, 477 (1985).
6. D.J. Parker, J.J. Hogan, J. Asher, Phys. Rev. C **35**, 161 (1987).
7. B. Bindu Kumar, S. Mukherjee, S. Chakraborty, B.S. Tomar, A. Goswami, S.B. Manohar, Phys. Rev. C **57**, 743 (1998).
8. B. Bindu Kumar, Anil Sharma, S. Mukherjee, S. Chakraborty, B.S. Tomar, A. Goswami, S.B. Manohar, S.K. Datta, Phys. Rev. C **59**, 2923 (1999).
9. Anil Sharma, B. Bindu Kumar, S. Mukherjee, S. Chakraborty, B.S. Tomar, A. Goswami, S.B. Manohar, J. Phys. G: Nucl. Part. Phys. **25**, 2289 (1999).
10. Anil Sharma, B. Bindu Kumar, S. Mukherjee, S. Chakraborty, B.S. Tomar, A. Goswami, S.B. Manohar, A.K. Sinha, S.K. Datta, Pramana J. Phys. **54**, 355 (2000).
11. L.C. Northcliffe, R.F. Schilling, At. Data Nucl. Data Tables A **7**, 233 (1970).
12. R.B. Firestone, V.S. Shirley, *Table of Isotopes*, 8th edition (Wiley, New York, 1996).
13. S. Chakraborty, B.S. Tomar, A. Goswami, G.K. Gubbi, S.B. Manohar, Anil Sharma, B. Bindu Kumar, S. Mukherjee, Nucl. Phys. A **678**, 355 (2000).
14. A. Gavron, Phys. Rev. C **21**, 230 (1985).
15. S.K. Kataria, V.S. Ramamurthy, S.K. Kapoor, Phys. Rev. C **18**, 549 (1978).
16. C.M. Perey, F.G. Perey, At. Data Nucl. Data Tables, **17**, 1 (1976).
17. P.M. Endt, Phys. Rev. Lett. **26**, 47 (1981).
18. R. Bass, Nucl. Phys. A **231**, 45 (1974).
19. G.N. Simonoff, J.M. Alexander, Phys. Rev. B **133**, 104 (1964).
20. T. Udagawa, T. Tamura, Phys. Rev. Lett. **45**, 1311 (1980).
21. J. Wilczynski, K. Siwek-Wilczynska, J. VanDriel, S. Gonggrijp, D.C.J.M. Hageman, R.V.F. Janssens, J. Lukasiak, R.H. Siemssen, S.Y. Van der Werf, Nucl. Phys. A **373**, 109 (1982).
22. M. Dasgupta, A. Navin, Y.K. Agrawal, C.V.K. Baba, H.C. Jain, M.L. Jhingan, A. Roy, Phys. Rev. Lett. **66**, 1414 (1991).